Structural and electrical properties of single crystalline and bi-crystalline ZnO thin films grown by molecular beam epitaxy*

Lu Zhong-Lin(路忠林)[a)b)c)†], Zou Wen-Qin(邹文琴)[a)], Xu Ming-Xiang(徐明祥)[c)], and Zhang Feng-Ming(张凤鸣)[a)]

[a)] *National Laboratory of Solid State Microstructure, and Department of Physics, Nanjing University, Nanjing* 210093, *China*
[b)] *Physics Department and Institute of Innovations and Advanced Studies (IIAS), National Cheng Kung University, Tainan* 701, *China*
[c)] *Department of Physics, Southeast University, Nanjing* 210096, *China*

(Received 8 September 2009; revised manuscript received 11 January 2010)

C-oriented ZnO epitaxial thin films are grown separately on the *a*-plane and *c*-plane sapphire substrates by using a molecular-beam epitaxy technique. In contrast to single crystalline ZnO films grown on *a*-plane sapphire, the films grown on *c*-plane sapphire are found to be bi-crystalline; some domains have a 30° rotation to reduce the large mismatch between the film and the substrate. The presence of these rotation domains in the bi-crystalline ZnO thin film causes much more carrier scatterings at the boundaries, leading to much lower mobility and smaller mean free path of the mobile carriers than those of the single crystalline one. In addition, the complex impedance spectra are also studied to identify relaxation mechanisms due to the domains and/or domain boundaries in both the single crystalline and bi-crystalline ZnO thin films.

Keywords: ZnO, grain boundaries, complex impedance spectra, single crystalline and bi-crystalline thin films

PACC: 6110M, 6170N 7280E, 7360L

1. Introduction

There has been a great deal of interest in ZnO semiconductor material for its wide prospects in optoelectronic applications, such as UV light emitters, sensors, displays, solar cells, etc., owing to its direct wide band gap of ~ 3.37 eV at room temperature.[1−4] Compared with GaN, another wide-gap semiconductor ($E_g \sim 3.4$ eV) which has been widely used for the production of light-emitting devices (LED), ZnO is considered to be more promising for optoelectronics applications due to the much simpler crystal-growth technology and the significant larger exciton binding energy (~ 60 meV) that would produce more efficient excitonic emission at room temperature.[5−7] In addition, ZnO has been also considered to be a promising candidate for spintronics applications.[8] The growth of ZnO thin films has been widely reported on various kinds of substrates by various deposition methods such as molecular-beam epitaxy (MBE),[9] chemical vapour deposition (CVD),[10] sputtering,[11] pulse laser deposition (PLD),[12] and spin coating.[13] Among these fabrication methods, MBE is the most precise technique allowing a fine control over the deposition procedure and the growth of high quality single crystalline ZnO thin films under appropriate growth conditions. Additionally, although high-quality ZnO substrates are available now, making homoepitaxy possible, the most popular substrate for growing ZnO thin films is sapphire (Al_2O_3) due to its low cost, availability as large-area wafers, and high thermal stability despite its poor structural and thermal match to ZnO.[14] In fact, due to the large lattice mismatch between the ZnO ($a = 3.250$ Å, $c = 5.213$ Å, 1 Å=0.1 nm) and the underlying sapphire ($a = 4.754$ Å, $c = 12.99$ Å) substrate, even after a 30° in-plane rotation to reduce the mismatch, as-grown ZnO films usually display large crystal mosaics, high density of defects and low mobil-

*Project partially supported by the National Natural Science Foundation of China (Grant No. 10804017), the Natural Science Foundation of Jiangsu Province of China (Grant No. BK2007118), the Research Fund for the Doctoral Program of Higher Education of China (Grant No. 20070286037), the Cyanine-Project Foundation of Jiangsu Province of China (Grant No. 1107020060), the Foundation for Climax Talents Plan in Six-Big Fields of Jiangsu Province of China (Grant No. 1107020070), and the New Century Excellent Talents in University (Grant No. NCET-05-0452).

†Corresponding author. E-mail: linzi077@163.com

© 2010 Chinese Physical Society and IOP Publishing Ltd

ities, making their use for optoelectronic applications a challenge.[15] Careful investigations on the growth, the structural and the electric properties of the ZnO thin films, as well as their correlations, are then necessary. In this paper, we report on the growth of single crystalline and bi-crystalline ZnO thin films on the *a*-plane and *c*-plane sapphire substrates, respectively, and their structural and electric properties are also studied.

2. Experiment

High-quality ZnO thin films with a thickness of 500 Å were prepared in an MBE system with a base pressure of 5×10^{-8} Pa on $Al_2O_3(11\bar{2}0)$ (*a*-plane) and $Al_2O_3(0001)$ (*c*-plane) substrates at 400 °C, respectively, under the same deposition conditions at a single growth run. High-purity (99.995%) ZnO was evaporated from an e-beam source. The sapphire substrates were degreased alternatively in ultrasonic acetone and methanol 3 times, and then inserted into the vacuum chamber. Prior to the film growth, the substrate surfaces were also cleaned by thermal annealing at 950 °C for 30 min. The typical growth pressure of the doped films was below 5×10^{-6} Pa and the deposition rate was about 0.02 Å/s. The structures and crystalline qualities of the films were determined by *in situ* high-energy electron diffraction (RHEED) and high-resolution x-ray diffraction (XRD) at the BL17B beamline of the Taiwan Light Source (TLS) in Hsinchu, Taiwan, China. Electrical transport including Hall measurements was carried out by using a four-terminal van der Pauw configuration in magnetic fields of up to 1 T. Complex impedance spectra were measured by using a Hewlett–Packard 4294A impedance analyzer with two point contacts and an oscillation voltage of 500 mV.

3. Results and discussion

For the film grown on a-plane sapphire, clear *c*-oriented ZnO $[11\bar{2}]$ streaky *in situ* RHEED patterns were observed (see the bottom inset in Fig. 1(a)), indicating the ZnO epilayer was grown in the Frank–Van der Merwe (FM) model with two-dimensional layer-by-layer growth.[16] It seems that the sample grown on *a*-plane sapphire is high-quality single crystalline (SC) ZnO thin film with an atomic flat surface morphology, which is suitable for multilayer devices. However, for the sample grown on *c*-plane sapphire, the spotty RHEED patterns showed twin crystal patterns, i.e. ZnO $[10\bar{1}0]$ patterns mixed in the ZnO $[11\bar{2}]$ patterns (see the top inset in Fig. 1(a)). This indicates that the sample is bi-crystalline (BC) ZnO thin film and contains two different domains that are rotated 30° with respect to each other in the *c*-plane, causing the film quality to degrade. All these can be well confirmed by XRD θ–2θ scans (Fig. 1(a)). The full width at half maximum (FWHM) of (0002) peak increases significantly from 0.17° for the SC sample to 0.31° for the BC one, suggesting poorer crystallinity with more defects formed in the BC ZnO film. Moreover, the in-plane azimuthal scans from a $(10\bar{1}1)$ plane of both the SC and BC samples were also performed to verify its in-plane crystalline characteristics as shown in Fig. 1(b).

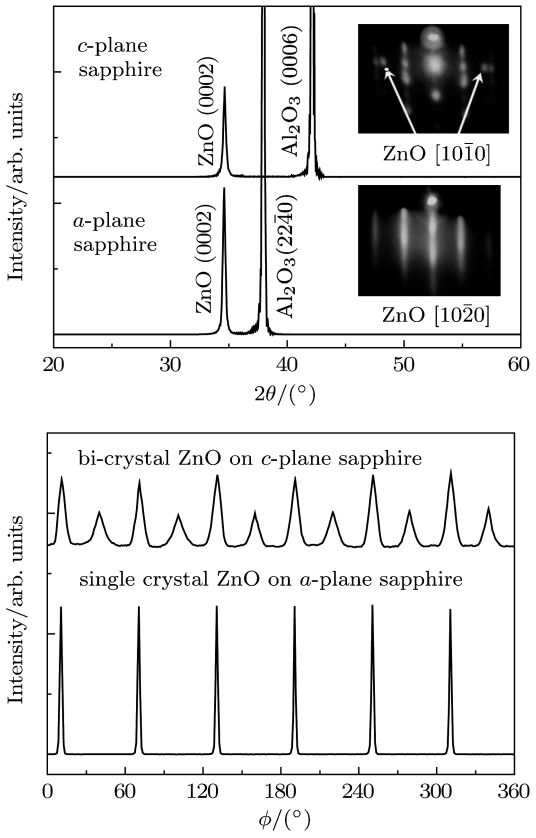


Fig. 1. (a) x-ray $\theta-2\theta$ scans and (b) ϕ scan from a $(10\bar{1}1)$ plane of the ZnO thin films grown on *a*-plane and *c*-plane sapphire substrates separately. The inset shows the typical RHEED patterns.

For the SC sample, the sixfold symmetry of the ZnO hexagonal structure crystal basal plane is clearly revealed by the six peaks separated by 60°, and the FWHW of the peaks is about 1.2°, revealing very good epitaxy. In contrast, it is noted that the twelve reflection peaks in the BC sample can be classified into a

high intensity set and a low intensity set each with a sixfold symmetry and are separated by 30° from each other, which also confirms the formation of twin domains in the BC ZnO sample.

In order to explore the growth mechanisms of the SC thin film and the BC ZnO thin film, the atom configurations of ZnO were schematically represented on the different surfaces of sapphire as shown in Fig. 2. For the ZnO epilayer on the *a*-plane of sapphire, because the ideal *a*-plane of sapphire is twofold symmetric while the ZnO *c* plane is sixfold symmetric, the two surfaces are essentially incommensurate except that

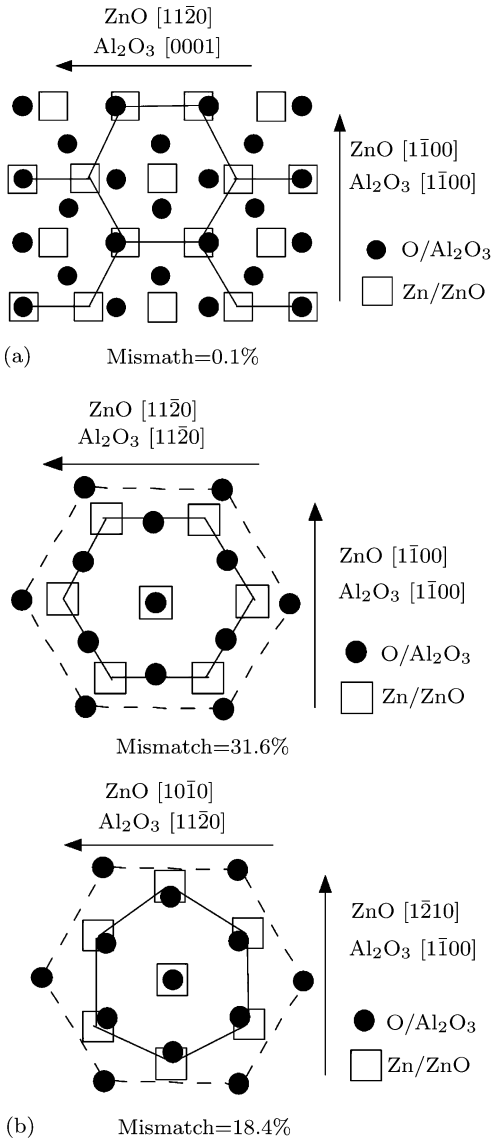


Fig. 2. Schematic diagrams of the atom positions for basal ZnO (0001) thin film grown on *a*-plane (a) and *c*-plane sapphire (b) separately.

the lattice constant of sapphire $c = 12.99$ Å, is almost 4 times the lattice constant of ZnO $a = 3.250$ Å (on the top of Fig. 2).[17] Accordingly, the ZnO *a* axis coincidentally matches along the sapphire [0001] direction, leading to the unique configuration in which the ZnO [0001]//sapphire [11$\bar{2}$0] and ZnO [11$\bar{2}$0]// sapphire [0001]. However, for the ZnO layer on the *c*-plane sapphire, in the idealized case shown in the middle of Fig. 2, the Zn atoms of ZnO would bond to the underlying sapphire O atoms to form a structure with a mismatch of 31.6%. The relationships of orientation between out-of-plane and in-plane are ZnO [0001]//sapphire [0001] and ZnO [11$\bar{2}$0]// sapphire [11$\bar{2}$0]. In order to reduce the mismatch, some domains may have a 30° in-plane rotation and the mismatch decreases to 18.4%, and this epitaxial relationship of ZnO grown on *c*-plane sapphire is shown in the bottom of Fig. 2. Accordingly, the relationships of orientation between out-of-plane and in-plane orientational are ZnO [0001]//sapphire [0001] and ZnO [10$\bar{1}$0]// sapphire [11$\bar{2}$0]. Hence, the ZnO thin film grown on *c*-plane sapphire is reasonable to be bicrystalline.

The electrical resistivities and the Hall effects of the SC and the BC ZnO samples were measured, and the data are shown in Table 1. Clearly, resistivity ρ of the BC ZnO sample (0.056 Ω·cm) is typically one order larger than that of the SC sample (0.0041 Ω·cm), because of a reduction in both carrier concentration n_c and Hall mobility μ. In fact, on one hand, for the BC sample the presence of domain boundaries can lead to the bending of inter-grain band and the forming of potential barriers,[18] which therefore contain a higher density of interfacial states and can trap more mobile carriers, leading to somewhat less n_c. On the other hand, these domain boundaries in the BC sample would cause much more carrier to scatter, thereby significantly reducing the carrier mobility by a factor of about ten. Moreover, the mean free path λ of the carrier at 300 K was estimated from equation $\lambda = \hbar(3\pi^2)^{1/3}/(n_c^{2/3}e^2\rho)$, where h is the Planck constant, and e the electron charge.[19] Clearly, compared with the relatively long λ (19.0 Å) of the SC sample, the λ value of the BC sample is much small and only about 1.75 Å, indicating that the carriers in BC sample are strongly localized due to much more carrier scatterings in the domain boundaries.

Table 1. Electrical parameters of SC and BC ZnO thin films at 300 K.

sample	$\rho/\Omega\cdot$cm	$\sigma/\Omega^{-1}\cdot$cm^{-1}	n_c/cm^{-3}	μ/cm$^2\cdot$V$^{-1}\cdot$s^{-1}	λ/Å
SC	4.1×10^{-3}	244	6.6×10^{19}	23.1	19.0
BC	5.6×10^{-2}	17.9	4.7×10^{19}	2.4	1.75

In order to further investigate the domains and/or the domain boundaries of the SC and BC samples, the radio frequency (RF) complex impedance method is employed herein. The RF impedance has been shown to be useful in unraveling the contributions of oxide structures (grains and grain boundaries), metal/oxide interfaces, etc.[20,21] Figures 3(a) and 3(b) show the real and the imaginary parts of complex impedance, $Z(f) = R(f) + \mathrm{i}\,X(f)$, of the SC and BC ZnO samples each as a function of frequency, respectively. For the SC sample, the real part of the complex impedance $R(f)$ just has a down step in a frequency range of $10^7 \sim 10^8$ Hz and the negative value of imaginary part $-X(f)$ seems to show a local maximum at a specific frequency above 10^8 Hz, which is considered as characteristic peak attributed to one type of electrical relaxation. In contrast, for the BC sample, there is another type of electrical relaxation corresponding to a specific frequency of about 10^5 Hz, most likely to be the contribution of domain boundaries.[22] The equivalent circuit composed of resistant (R) and capacitance (C) elements is utilized in the analysis of the measured ac impedance spectra.[23] Elements R and C are in parallel and used to describe an intermediate step of $R(f)$, corresponding to a local maximum of $-X(f)$. Based on our impedance results, a set of parallel RC component and two sets of parallel RC components in series, are employed to model the complex impedance spectra of the SC and BC ZnO samples, respectively: $\rho*(f) = (\rho_{\mathrm{g}}^{-1} + \mathrm{i}\,2\pi f C_{\mathrm{g}})^{-1}$ for the SC sample and $\rho*(f) = (\rho_{\mathrm{g}}^{-1} + \mathrm{i}\,2\pi f C_{\mathrm{g}})^{-1} + (\rho_{\mathrm{gb}}^{-1} + \mathrm{i}\,2\pi f C_{\mathrm{gb}})^{-1}$ for the BC sample, where ρ_{g} and C_{g} represent the resistivity and the capacitance of ZnO domain contribution, and ρ_{gb} and C_{gb} are the resistivity and the capacitance of ZnO domain boundaries, respectively. The dash lines in Fig. 3 are obtained by the best fitting of the experimental data, which reveal good agreement between the equivalent circuit model and the impedance spectra. The resistivity ρ and the relaxation time ($\tau = \rho C$), which is an intrinsic characteristic property of the materials independent of the sample geometry, can be obtained from the fitting parameters as shown in Table 2.

Table 2. Fitted results of resistivity (ρ) and relaxation time (τ) for the complex impedance spectra as shown in Fig. 3.

sample	$\rho_{\mathrm{g}}/\Omega\cdot$cm	τ_{g}/s	$\rho_{\mathrm{gb}}/\Omega\cdot$cm	τ_{gb}/s
SC	4.1×10^{-3}	6.9×0^{-10}	–	–
BC	1.1×10^{-2}	1.3×10^{-9}	4.5×10^{-2}	1.2×10^{-6}

Clearly, resistivity ρ_{g} of the BC ZnO matrix is larger than that of the SC ZnO matrix as expected, due to poorer crystallinity with more defects because of the large mismatch. Moreover, the slower τ_{g} of the BC ZnO matrix also confirms the presence of more structural defects in it. In addition, for the BC sample, the value of ρ_{gb} is much larger than that of ρ_{g}, revealing much more defects generated at the boundaries for carrier scattering, which is well consistent with the Hall measurements.

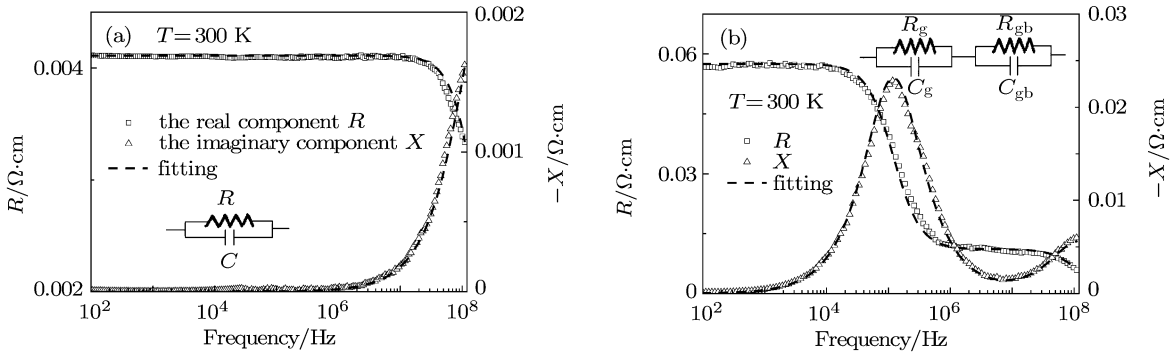


Fig. 3. Real part ($R(f)$) and imaginary part ($-X(f)$) of complex impedance of the SC (a) and BC ZnO thin films (b), each as a function of frequency. The dash lines represent the best fitting results by the equivalent circuit equations.

4. Conclusions

We grow ZnO thin films separately on the a-plane and c-plane sapphire substrates by using MBE. It is found that the ZnO film grown on a-plane sapphire is single crystalline, while the film grown on c-plane sapphire is bi-crystalline ZnO with some domains having a 30° rotation to reduce the mismatch. The presence of these rotation domains in the bi-crystalline ZnO thin film causes much more carrier scatterings at the boundaries, leading to much lower mobility and a smaller mean free path of the mobile carriers. The complex impedance spectra confirm the dominant role of domain boundary scattering in determining the resistivity of the bi-crystalline ZnO thin film. Our studies are useful for understanding the growth mechanisms and the electric properties of ZnO thin films.

References

[1] Cho S, Ma J, Kim Y, Sun Y, Wong G K L and Ketterson J B 1999 *Appl. Phys. Lett.* **75** 2761

[2] Cao H, Xu J Y, Seeling E W and Chang R P H 2000 *Phys. Rev. Lett.* **84** 5584

[3] Tsukazaki A, Ohotmo A, Onuma T, Ohtani M, Makino T, Sumiya M, Ohtani K, Chichibu Shigefusa F, Fuke S, Segawa Y, Ohno H, Koinuma H and Kawasaki M 2005 *Nat. Mater.* **4** 42

[4] Sun H, Zhang Q F and Wu J L 2007 *Acta Phys. Sin.* **56** 3479 (in Chinese)

[5] Look D C, Reynolds, Sizelove J R, Jones R L, Litton C W, Cantwell G and Harsch W C 1998 *Solid State Commun.* **105** 399

[6] Norton D P, Heo Y W, Ivill M P, Ip K, Pearton S J, Chisholm M F and Steiner T 2004 *Mater. Today* **7** 34

[7] Service 1997 *Science* **276** 895

[8] Dietl T, Ohno H, Matsukura F, Cubert J and Ferrand D 2000 *Science* **287** 1019

[9] Chen Y, Ko H J, Hong S K and Yao T 2000 *Appl. Phys. Lett.* **76** 559

[10] Cheng Z Q, Liu M H, Liu Y P, Chen W, Luo Z Q and Hu X W 2009 *Acta Phys. Sin.* **58** 4260 (in Chinese)

[11] Liu M, Liu Z W, Gu J F, Qin F W, Ma C Y and Zhang Q Y 2008 *Acta Phys. Sin.* **57** 1133 (in Chinese)

[12] Zhou X, Wang S Q, Lian G J and Xiong G C 2006 *Chin. Phys.* **15** 0199

[13] Wang Z J, Song L J, Li S C, Lu Y M, Tian Y X, Liu J Y and Wang L Y 2006 *Chin. Phys.* **15** 2710

[14] Özgür Ü, Alivov Ya I, Liu C, Teke A, Reshchikov M A, Doğan S, Avrutin V, Cho S J and Morkoç H 2005 *J. Appl. Phys.* **98** 041301

[15] Hong N H, Brize V and Sakai J 2005 *Appl. Phys. Lett.* **86** 082505

[16] Cao Q, Deng J X, Liu G L, Chen Y X, Yan S S and Mei L M 2007 *Chin. Phys. Lett.* **24** 2951

[17] Fons P, Iwata K, Yamada A, Matsubara K, Niki S, Nakahara K, Tanabe T and Takasu H 2000 *Appl. Phys. Lett.* **77** 1801

[18] Orton J W and Powell M J 1980 *Rep. Prog. Phys.* **43** 1263

[19] Behan A J, Mokhtari A, Blythe H J, Score D, Xu X H, Neal J R, Fox A M and Gehring G A 2008 *Phys. Rev. Lett.* **100** 047206

[20] Shao R, Kalinin S V and Bonnell D A 2003 *Appl. Phys. Lett.* **82** 1869

[21] Ortega N, Kumar A, Bhattacharya P, Majumder S B and Katiyar R S 2008 *Phys. Rev.* B **77** 014111

[22] Hsu H S, Huang J C A, Chen S F and Liu C P 2007 *Appl. Phys. Lett.* **90** 102506

[23] Hsu C Y, Huang J C A, Lee Y H, Chen S F, Liu C P, Sun S J and Tzeng Yonhua 2009 *Appl. Phys. Lett.* **94** 052504